Molecular Neurobiology (2019) 56:6436–6450
https://doi.org/10.1007/s12035-019-1526-1

Perineuronal Nets Restrict the Induction of Long-Term Depression in the Mouse Hippocampal CA1 Region

Guan Hock Khoo [1] · Yu-Ting Lin [1,2] · Tsung-Chih Tsai [2] · Kuei-Sen Hsu [1,2]

Received: 1 November 2018 / Accepted: 8 February 2019 / Published online: 2 March 2019

Abstract

Long-term depression (LTD) of synaptic efficacy is widely regarded as a cellular basis of learning and memory. The magnitude of hippocampal CA1 LTD induced by low-frequency stimulation (LFS) declines with age, but the mechanisms involved remain poorly understood. Perineuronal nets (PNNs) are specialized extracellular matrix structures that function in dampening synaptic plasticity during postnatal development, suggesting that PNN formation may restrict LTD induction in the adult hippocampus. Here, we show that PNNs tightly enwrap a subpopulation of parvalbumin (PV) interneurons in the hippocampal CA1 region and enzymatic removal of PNNs with the chondroitinase ABC alters the excitatory/inhibitory synaptic balance toward more excitation and restores the ability of LFS to induce an *N*-methyl-D-aspartate receptor-dependent LTD at Schaffer collateral-CA1 synapses in slices from male adult mice. Early interference with depolarizing GABA with Na^+-K^+-$2Cl^-$ cotransporter inhibitor bumetanide impairs the maturation of PNNs and enhances LTD induction. These results provide novel insights into a previously unrecognized role for PNNs around PV interneurons in restricting long-term synaptic plasticity at excitatory synapses on hippocampal CA1 neurons in adulthood.

Keywords Perineuronal nets · Long-term depression · Excitatory/inhibitory synaptic balance · Parvalbumin interneurons · Hippocampus

Introduction

Long-term depression (LTD) is a persistent activity-dependent reduction in synaptic efficacy that, together with its counterpart, long-term potentiation (LTP), has long been implicated in information storage and adaptation to external stimuli [1–3]. Over the past decades, LTD received much less attention than LTP among those who study synaptic plasticity. While LTD can be induced in many brain regions, much of our current understanding of the properties and its functional relevance comes from studies in the hippocampus. In the hippocampus, LTD can be experimentally induced by several different types of electrical and pharmacological stimulation protocols [1, 4, 5]. The most commonly used protocol for inducing LTD involves prolonged low-frequency stimulation (LFS) at 0.5–5 Hz. In the hippocampal CA1 region, LFS-induced LTD (LFS-LTD) requires the activation of *N*-methyl-D-aspartate receptors (NMDARs), a rise in postsynaptic intracellular Ca^{2+}, and through consequential activation of serine-threonine protein phosphatase cascades [6, 7]. Despite considerable progress in understanding the cellular and molecular mechanisms underlying LTD, it was intriguing to find that LTD is difficult to elicit and less robust in hippocampal slices from adult animals when compared to slices from their young counterparts [8–13]. However, the mechanisms underlying the age-related decline in the magnitude of LTD remain elusive.

Perineuronal nets (PNNs) are lattice-like extracellular matrix structures that wrap around the soma and proximal dendrites of subpopulations of neurons throughout the brain and spinal cord [14–16]. PNNs are formed during postnatal development and completed by early adulthood [17]. The importance of PNNs is highlighted by the fact that the emergence of PNNs coincides with closure of the critical period plasticity within the visual, motor, and somatosensory systems [17–20], suggesting a possible role of PNNs in restricting brain plasticity and stabilizing neural network. Parvalbumin (PV)-expressing interneurons are the predominant neuronal subtype that is enveloped by PNNs.

✉ Kuei-Sen Hsu
richard@mail.ncku.edu.tw

[1] Department of Pharmacology, College of Medicine, National Cheng Kung University, No. 1, University Rd., Tainan City 70101, Taiwan

[2] Institute of Basic Medical Sciences, College of Medicine, National Cheng Kung University, Tainan 70101, Taiwan

The role of PNNs in the regulation of PV interneuron function has not reached a consensus. Degradation of PNNs has been shown to increase [21, 22] or decrease [23] the intrinsic excitability of PV interneurons. PNNs have also been shown to control synaptic plasticity in the amygdala and hippocampus. In the amygdala, PNN deposition is followed by fear memory persistence, and conversely, disruption of PNNs by chondroitinase ABC (ChABC) renders fear memories susceptible to erasure [24]. Additionally, in the hippocampus, PNNs have been shown to modulate LTP at Schaffer collateral-CA1 synapses [25, 26] and contribute to contextual fear memory [26], as well as suppress LTP at excitatory synapses on CA2 pyramidal neurons [27]. These findings strongly imply a potential role for PNNs in regulating LTD induction, but direct and causal evidence for this association is currently unavailable. Therefore, in the present study, we hypothesized that PNNs may act as a molecular brake on LTD induction and that the progressive developmental increase in PNNs may be associated with age-related decrease in the magnitude of LTD at Schaffer collateral-CA1 synapses. Although γ-aminobutyric acid (GABA) is a major inhibitory neurotransmitter in the adult brain, GABA excites immature neurons due to high expression of the Na^+-K^+-$2Cl^-$ cotransporter (NKCC1) in the developing brain [28]. GABA-mediated depolarization has been implicated in a series of developing processes, including neuronal migration and morphological differentiation, and the plasticity of neuronal circuits [29, 30]. Previous work demonstrated that blocking early GABA-mediated depolarization with selective NKCC1 antagonist bumetanide results in lasting disruption of cortical excitatory synapse formation [31]. Interestingly, a recent study indicated that early bumetanide treatment impairs PNN development around PV interneurons and prolongs critical period plasticity in the rat visual cortex [32]. On the basis of these observations, we also hypothesized that bumetanide treatment during early postnatal development may affect the maturation of PNNs, which may then alter the critical period for LTD induction. Here, our results demonstrate, for the first time, that PNNs function to restrict CA1 LTD induction in adulthood and that PNN disruption reinstates juvenile-like states of synaptic plasticity. In addition, the effect of PNNs on LTD induction emerged from maintaining excitation/inhibition synaptic balance in CA1 network of the hippocampus. Moreover, early-life bumetanide treatment impairs the maturation of PNNs and enhances LTD induction in adult slices.

Materials and Methods

Animals

Young (P14-28) and adult (P56-84) male C57BL/6 mice were used in experiments. Mice were housed in groups of four under a 12-h light/dark cycle (lights off at 7:00 P.M.) with access to food and drinking water ad libitum. All experimental procedures were conducted in accordance with the National Institutes of Health guidelines for the care and use of laboratory animals and were approved by the Institutional Animal Care and Use Committee of National Cheng Kung University. In early-life bumetanide treatment experiments, male littermates were injected intraperitoneally twice daily, from P3 to P8, with vehicle [0.01% dimethyl sulfoxide (DMSO) in physiological solution] or bumetanide (0.2 mg/kg body weight; Sigma-Aldrich, Saint Louis, MO), according to previously described treatment regimen [32].

Hippocampal Slice Preparations and Electrophysiological Recordings

Acute hippocampal slices were prepared using standard procedures as described previously [33]. Mice were deeply anesthetized with 5% isoflurane and sacrificed by decapitation. The brain was removed and quickly placed in ice-cold oxygenated sucrose cutting solution containing the following (in mM): 234 sucrose, 2.5 KCl, 0.5 $CaCl_2$, 7 $MgCl_2$, 25 $NaHCO_3$, 1.25 NaH_2PO_4, and 11 glucose at pH 7.3–7.4 and equilibrated with 95% O_2–5% CO_2. Coronal slices containing the hippocampus (250 or 400 μm) were prepared using a vibrating microtome (VT1200S; Leica Biosystems, Wetzlar, Germany) and immediately transferred to a holding chamber of artificial cerebrospinal fluid (aCSF) containing the following (in mM): 117 NaCl, 4.7 KCl, 2.5 $CaCl_2$, 1.2 $MgCl_2$, 25 $NaHCO_3$, 1.2 NaH_2PO_4, and 11 glucose at pH 7.3–7.4 and equilibrated with 95% O_2–5% CO_2 and then kept at room temperature (~25 °C) for at least 1 h before starting recordings. For ChABC treatment experiments, slices were incubated with vehicle [0.1% bovine serum albumin (BSA)] or ChABC (0.2 U/ml in 0.1% BSA; Sigma-Aldrich catalog# C2905) for at least 2 h at 37 °C before being transferred to the recording chamber, according to previously described procedure [25].

For extracellular field potential recordings, one slice was transferred to a submersion-type recording chamber and continuously perfused with oxygenated aCSF at a flow rate of 2–3 ml/min at ~32 °C on a fixed stage. The extracellular field potential recordings were carried out using an Axoclamp-2B amplifier (Molecular Devices, San José, CA). Microelectrodes were pulled from microfiber-containing glass capillary tubings (outer diameter = 1.0 mm) on a Brown-Flaming electrode puller (Sutter Instruments, Novato, CA) and were filled with 1 M NaCl. The responses were low-pass-filtered at 2 kHz, digitally sampled at 10 kHz using a Digidata 1320A (Molecular Devices), and analyzed with pCLAMP 8.0 software (Molecular Devices). Field excitatory postsynaptic potentials (fEPSPs) were evoked by electrical stimulation to Schaffer collateral/commissural fibers in the stratum radiatum of the CA1 area with a bipolar tungsten-stimulating electrode at the baseline frequency of 0.033 Hz.

The stimulation strength was adjusted to elicit a response having amplitude that was 30–40% of the maximum spike-free response. The slope of fEPSP was measured from approximately 20–70% of the rising phase using the least squares regression. Paired-pulse facilitation (PPF) was assessed by using a succession of paired pulses separated by intervals of 20, 40, 60, 80, 100, and 200 ms. LTD was induced by application of LFS at 1 Hz for 15 min (900 pulses), paired-pulse LFS (PP-LFS) at 1 Hz for 15 min (900 paired pulses, 40 ms interpulse interval), (S)-3,5-dihydroxyphenylglycine (DHPG, 50 μM; Tocris Bioscience, Bristol, UK) for 5 min, or NMDA (15 μM; Tocris) for 3 min. The magnitude of LTD was calculated as percentage of change of fEPSP slope 50–60 min after LTD induction compared to baseline fEPSP (10 min before LTD induction).

Whole-cell patch-clamp recordings were made from visualized pyramidal neurons in the CA1 region of hippocampal slices using an Axopatch 200B amplifier (Molecular Devices). Data acquisition and analysis were performed using a digitizer (Digidata 1440A) and pCLAMP 9 software (Molecular Devices). Patch pipettes (3–6 MΩ) were filled with an intracellular recording solution containing the following (in mM): 130 $CsMeSO_4$, 8 CsCl, 1 $MgCl_2$, 0.3 EGTA, 10 HEPES, 4 Mg-ATP, 0.3 Na-GTP, 10 Na-phosphocreatine, and 1 QX-314 (pH 7.2 adjusted with CsOH; 280–290 mOsm). To evoke perisomatic inhibition, a bipolar-stimulating electrode was placed in the middle of the stratum pyramidale (SP) of CA1 region 200 μm away from the recorded cell. To evoke dendritic inhibition, the stimulating electrode was placed in the stratum radiatum (SR), 200–300 μm away from the recorded cell. All stimulation was conducted at 0.1 Hz to avoid inducing synaptic plasticity. Excitatory postsynaptic current/inhibitory postsynaptic current (EPSC/IPSC) ratio was calculated as the peak EPSC at − 65 mV divided by the IPSC amplitude at 0 mV. A total of 20 recording events with intervals of 30 s at each holding potential were used for analysis. For miniature inhibitory postsynaptic current (mIPSC) recordings, $CsMeSO_4$ was replaced with CsCl in the intracellular recording solution and tetrodotoxin (TTX, 0.5 μM; Sigma-Aldrich), 6-cyano-7-nitroquinoxaline-2,3-dione (CNQX, 20 μM; Tocris), and D-2-amino-5-phosphonopentanoic acid (APV, 50 μM; Tocris) were added to the bath. mIPSCs were recorded from CA1 pyramidal neurons held in voltage-clamp mode at a holding potential of − 60 mV and analyzed off-line using a commercially available software (Mini Analysis 4.3; Synaptosoft, Leonia, NJ) as previously described [34]. Bicuculline methiodide (20 μM; Tocris) was routinely applied at the end of the recording to verify that the mIPSCs were exclusively mediated by $GABA_A$ receptors. Means were calculated from 3-min epochs recorded. Detection threshold for analysis was set at three times the root mean square of the background noise, and each event was further confirmed by visual inspection after detection. To assess cell stability, series and input resistances were continuously monitored throughout the experiment with a 5-mV depolarizing step given after every afferent stimulus and data were excluded from analysis if resistance changed by more than 20%.

Immunohistochemistry

Mice were deeply anesthetized with a mixture of Zoletil (50 mg/kg; Virbac, Carros, France) and Rompun (0.5 mg/kg; Bayer, Leverkusen, Germany), and were perfused transcardially with 4% paraformaldehyde (PFA) in 0.1 M phosphate-buffered saline (PBS), pH 7.4. After the perfusion, brains were rapidly removed, fixed in 4% PFA for 24 h at 4 °C, and then equilibrated in 30% sucrose for 48 h at 4 °C before slicing. Coronal brain slices (20 μm) containing the hippocampus were washed with 0.4% Triton X-100-containing PBS and then incubated in blocking solution containing 3% goat serum in PBS. After this, sections were incubated in the primary antibodies against NeuN (1:200; Millipore catalog# MAB377, RRID:AB_2298772, Darmstadt, Germany), calcium/calmodulin-dependent protein kinase IIα (CaMKIIα, 1:500; Novas Biologicals catalog# NB100-81830, RRID:AB_1145020, Littleton, CO), glutamic acid decarboxylase 67 (GAD67, 1:1000; Millipore catalog# MAB5406, RRID:AB_2278725), parvalbumin (PV, 1:1000; Millipore catalog# MAB1572, RRID:AB_2174013), or *Wisteria floribunda* agglutinin (WFA, 1:1000; Vector laboratories catalog# B-1355, RRID:AB_2336874, Burlingame, CA). Finally, sections were washed three times with 0.4% Triton X-100 in PBS and incubated in secondary Alexa Fluor 488 (Invitrogen Molecular Probes, catalog# A150077, Eugene, OR) or Alexa Fluor 568 antibodies (Invitrogen Molecular Probes, catalog# A10037) for 2 h at room temperature. After being washed with PBS, sections were mounted with ProLong Gold Antifade Reagent (Invitrogen Molecular Probes) with or without 4′,6-diamidino-2-phenylindole (DAPI; Vector Laboratories). Images were acquired on an Olympus FluoView FV1000 confocal microscope (Olympus, Tokyo, Japan) with sequential acquisition setting at a resolution of 1024 × 1024 pixels, z-stack with 15–20 optical sections. All images were analyzed by NIH ImageJ software and all the parameters used were kept consistent during capturing. For the quantification of PNN+ and PV+ neurons, the dorsal hippocampal CA1 was analyzed at − 1.94 to − 2.18 mm from bregma as described previously [35]. Three sections per mouse were acquired and analyzed. The data per mouse was the average of the sections. All counting was performed in a blind manner.

Statistical Analysis

No statistical methods were used to predetermine sample size, but our sample sizes were based on previous work of a similar

nature by our laboratory [36, 37]. The results are presented as mean ± SEM. All statistical analyses were performed using the GraphPad Prism 6 software (RRID:SCR_000306). To compare the difference between the two population means, we first determined whether the data were normally distributed using the Shapiro-Wilk test. The significance of any difference between two groups was calculated using the unpaired two-tailed Student *t* test. One-way or two-way repeated measures ANOVA tests were used for multiple groups' comparison and Bonferroni's post hoc analyses were used to assess the significance between groups. Because the data of LTD magnitudes was not normally distributed, the Mann-Whitney *U* test was used to compare differences between two independent groups. *N* represents the number of slices or animals used. Values of $p < 0.05$ were considered significant.

Results

PNNs Mainly Enwrap a Subpopulation of Parvalbumin-Expressing Interneurons

We initially sought to examine the distribution of PNNs and the identity of PNN-enwrapped cells in the hippocampal CA1 region of adult mice. PNN-enwrapped cells, as detected by WFA labeling [25], were found predominantly in the stratum oriens (SO) and SP of the CA1 region. Double immunofluorescent staining with the neuronal marker NeuN revealed that nearly all PNN-enwrapped cells were positive for NeuN (~ 95.6%), indicating that these cells were neurons (Fig. 1a, c). To determine the identity of PNN-enwrapped neurons, double immunofluorescent staining was performed with antibody against CaMKIIα, a marker of excitatory neurons. Immunoreactivity for CaMKIIα was not detected at all PNN-enwrapped neurons (Fig. 1a, c). In contrast, we observed that the large majority (~ 90.5%) of PNN-enwrapped neurons express GAD67, a marker of GABAergic neurons (Fig. 1b, c). Moreover, consistent with previous work [22, 38], the vast majority (89.8 ± 4.8%) of PNN-enwrapped neurons were immunopositive for PV; however, only 40.3 ± 5.6% of PV-expressing (PV+) neurons were labeled with WFA (Fig. 1d). The density of WFA + PV+ neurons was highest in the SP, less in the SO and SR, but not in the stratum lacunosum-moleculare (SLM) (Fig. 1e). These results indicate that PNNs are predominantly expressed around a subpopulation of PV+ GABAergic interneurons in the hippocampal CA1 region.

An Inverse Correlation Between PNNs and the Magnitude of LTD

To explore the interaction between PNNs and LTD induction in early life, we measured the expression of PNNs and the magnitude of LTD in the hippocampal CA1 region of mice at three different developmental stages. If an increase in PNNs is a critical contributor to dampen LTD, then the time course of these changes should directly overlap in time with changes in LTD magnitude. In agreement with previous findings [39, 40], we observed that the densities of PV+ (Fig. 2a, b) and WFA+ neurons (Fig. 2a, c) in the CA1 SP and SO increased gradually with age during early postnatal development. Accordingly, there was a progressive increase in the density of WFA + PV+ neurons across postnatal age from postnatal day (P) 14 to P28 (Fig. 2a, d). To assess age-related alterations in LTD induction, we chose a prolonged LFS (1 Hz for 15 min) protocol particularly efficient in inducing robust LTD at Schaffer collateral-CA1 synapses in hippocampal slices from younger animals [12, 41]. As expected, a significant age-related decrease in the magnitude of CA1 LTD (50–60 min after the end of LFS) was observed (one-way ANOVA, $F_{(2,17)} = 25.23$, $p < 0.0001$), with 33.2 ± 3.5% depression in P14 pups, 23.8 ± 2.6% in P21 juveniles, and 5.8 ± 1.4% in P28 young adults (Fig. 2e, f). Moreover, a statistically significant inverse correlation was observed between the density of WFA + PV+ neurons and the magnitude of LFS-LTD ($r = 0.99$, $p = 0.045$; Fig. 2g).

PNNs Restrict LFS-Induced LTD

Having observed an inverse relationship between PNNs and the magnitude of LFS-LTD during early postnatal development, we next asked whether PNNs act to restrict LFS-LTD induction in the hippocampal CA1 region of adult mice. To test this, we degraded PNNs with the enzyme ChABC, which digested and removed glycosaminoglycan chains from the core proteins in PNNs [42], in acute hippocampal slices from adult mice (P56-P84) and attempted to induce LFS-LTD at Schaffer collateral-CA1 synapses. Enzymatically treated slices were morphologically and functionally intact (on the basis of normal action potential firing, Fig. 6a). As demonstrated previously [25], we found that 2-h treatment of slices with ChABC (0.2 U/ml in 0.1% BSA) ablated WFA-labeled PV+ neurons in the hippocampal CA1 region (Fig. 3a). Treatment of slices with ChABC did not affect basal synaptic transmission because the stimulus-response curves for fEPSPs were similar between vehicle (0.1% BSA)- and ChABC-treated slices (Fig. 3b). In addition, we found no significant difference between vehicle- and ChABC-treated slices in PPF of fEPSPs, an indirect measure of presynaptic release probability, at any of the interpulse intervals examined (Fig. 3c). As reported previously for untreated slices [12, 41], LFS at 1 Hz for 15 min failed to elicit a reliable LTD at Schaffer collateral-CA1 synapses in vehicle-treated slices. However, a 2-h incubation with ChABC enabled LTD induction in slices from adult mice (Fig. 3d). Notably, LTD in slices treated with ChABC was significantly greater than LTD in slices treated with vehicle ($p = 0.04$, Mann-Whitney *U* test; Fig. 3g). To more thoroughly

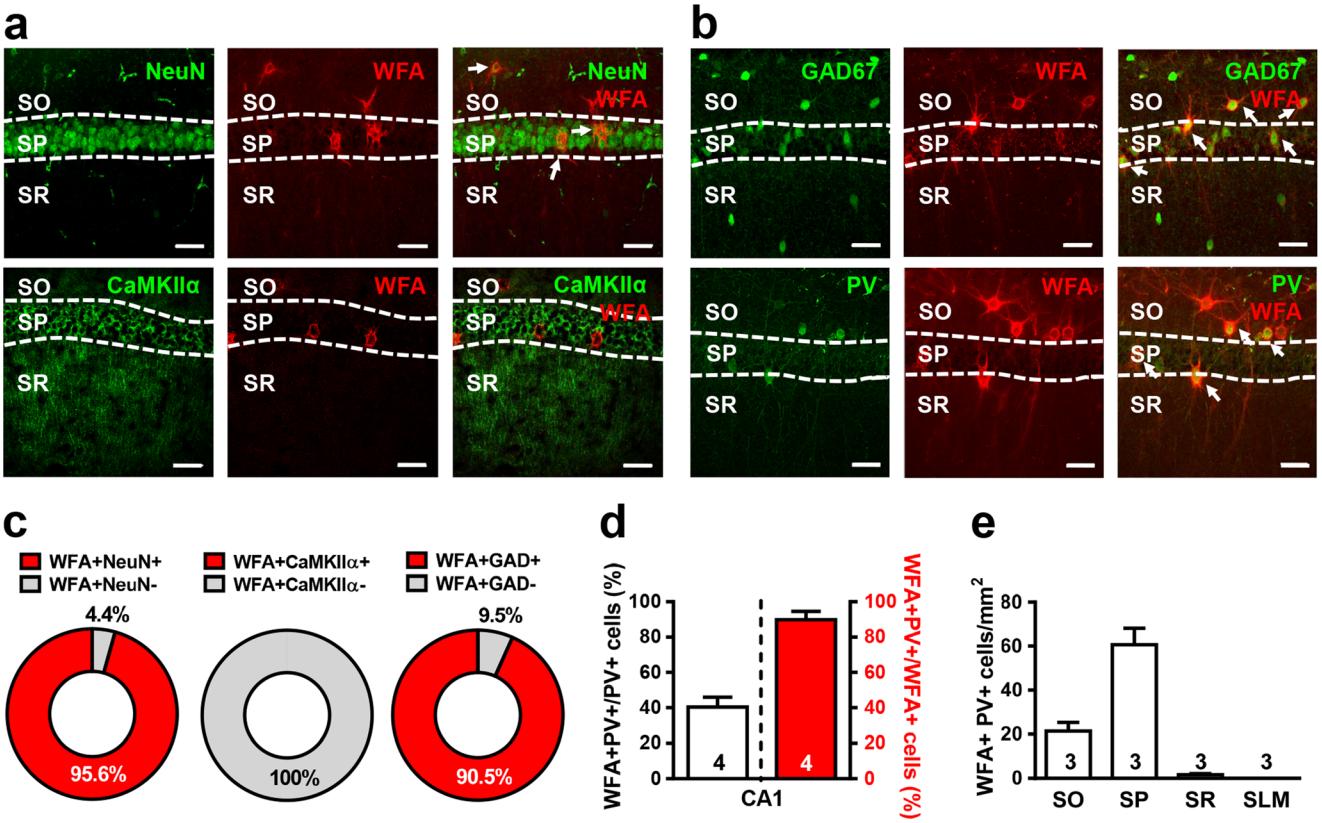

Fig. 1 Distribution of PNNs in the hippocampal CA1 region of adult mice. **a**, **b** Double-labeled confocal immunofluorescence images showing the colocalization of WFA (red) expression with **a** NeuN (green) and CaMKIIα (green), and **b** GAD67 (green) and PV (green) in the hippocampal CA1 region of adult (P56) mice. Arrows point to double-labeled cells. SO, SP, and SR denote the stratum oriens, stratum pyramidale, and stratum radiatum, respectively. Scale bar, 40 μm. **c** Pie charts showing the percentage of WFA-labeling cells that expressed NeuN, CaMKIIα, and GAD67 in the hippocampal CA1 region ($n = 4$ mice for each group). **d** Bar graph showing the percentage of WFA + PV+ neurons in total PV+ neurons (left, open bar) and the percentage of WFA + PV+ neurons in total WFA+ neurons (right, red bar) ($n = 4$ mice). **e** Bar graph showing the density of WFA + PV+ neurons in the SO, SP, SR, and stratum lacunosum-moleculare (SLM) of the CA1 region ($n = 3$ mice). Data represent the mean ± SEM

examine whether PNNs also regulate the induction of other forms of CA1 LTD induced by different stimulation protocols, we recorded LTD induced by group I metabotropic glutamate receptor (mGluR) agonist DHPG and PP-LFS, respectively, in slices that were treated with vehicle or ChABC. As shown in Fig. 3e, bath application of DHPG (50 μM) for 5 min induced a reliable LTD of fEPSPs. We detected no significant difference in the magnitude of DHPG-induced LTD between vehicle- and ChABC-treated slices (Fig. 3g). Moreover, unlike that in LFS-LTD, there was no age-related loss of LTD induced by PP-LFS (Fig. 3f). There was no difference in the magnitude of PP-LFS-induced LTD between vehicle- and ChABC-treated slices (Fig. 3g). Collectively, these results indicate that PNNs specifically restrict LFS-LTD at mature Schaffer collateral to CA1 synapses.

Mechanisms Underlying the Induction of LFS-LTD in ChABC-Treated Slices

We then set out to uncover the possible mechanism underlying LFS-induced LTD in ChABC-treated slices from adult mice. In slices from young animals, it is well known that hippocampal CA1 LFS-LTD is dependent on the activation of NMDARs [6, 7]. Consistent with a requirement for NMDAR activation, LFS-LTD in ChABC-treated slices from adult mice was no longer observed in the presence of the broad-spectrum NMDAR antagonist APV (50 μM) (Fig. 4a, f) or the NMDAR glycine site antagonist L689,560 (10 μM; Tocris) (Fig. 4b, f). Neither APV nor L689,560 treatments affected the effect of LFS on synaptic transmission in vehicle-treated slices. There is also evidence indicating that LTD can be induced in hippocampal slices by direct application of NMDA through the activation of both synaptic and extrasynaptic NMDARs [43]. As chemically induced LTD shares common saturable expression mechanism(s) with LFS-LTD in the hippocampal CA1 region [1, 43], we investigated the effect of ChABC on NMDA-induced LTD. However, in contrast to what we observed in LFS-LTD, we found no significant difference in the magnitude of NMDA-induced LTD between vehicle- and ChABC-treated slices (Fig. 4c, f). LFS-LTD was still observed in ChABC-treated

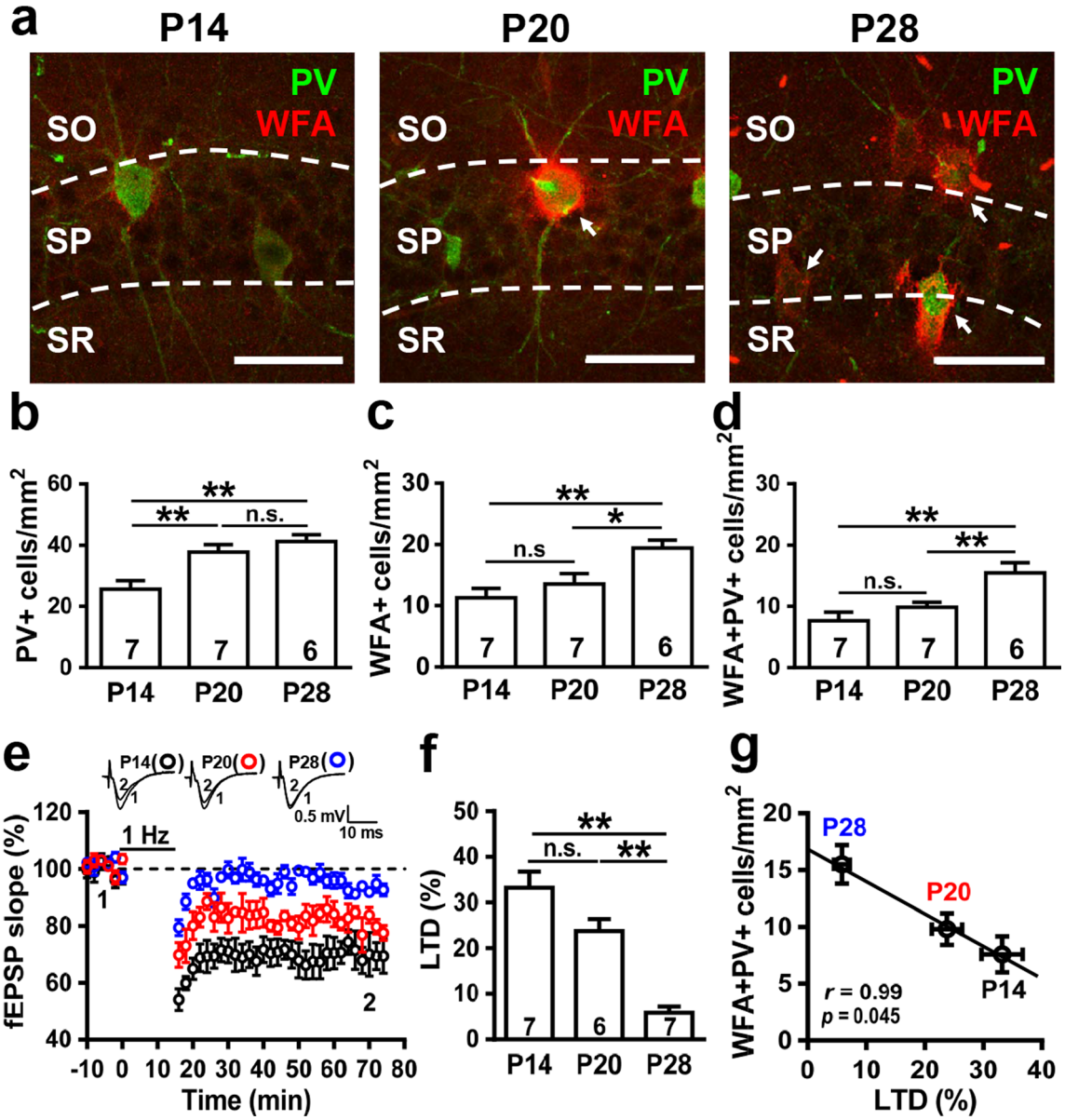

Fig. 2 An inverse correlation between PNNs and the magnitude of LFS-LTD. **a** Representative immunofluorescence images showing the expression of WFA + PV+ neurons in the CA1 region of mouse hippocampus at P14, P20, and P28. Arrows point to double-labeled cells. Scale bar, 40 μm. **b**–**d** Bar graph showing the densities of **b** PV+ (one-way ANOVA, $F_{(2,17)} = 10.62$, $p = 0.001$, $n = 7, 7, 6$); **c** WFA+ (one-way ANOVA, $F_{(2,17)} = 6.97$, $p = 0.006$, $n = 7, 7, 6$); and **d** WFA + PV+ neurons (one-way ANOVA, $F_{(2,17)} = 8.99$, $p = 0.002$, $n = 7, 7, 6$) in the CA1 region of mouse hippocampus at P14, P20, and P28. **e** The developmental profile of LFS-LTD. Upper panel: representative traces of fEPSPs were taken at the time indicated by number. Summary of experiments showing the induction of hippocampal CA1 LTD by a prolonged LFS (1 Hz for 15 min) at Schaffer collateral-CA1 synapses in slices from P14, P20, and P28 mice. *Dash lines* show level of baseline. **f** Summary bar graphs comparing averaged magnitudes of LFS-LTD in slices from P14, P20, and P28 mice. The magnitude of LTD was measured at 50–60 min after LFS (Mann-Whitney *U* test, P14 versus P20: $p = 0.05$; P14 versus P28: $p = 0.001$; P20 versus P28: $p = 0.002$, $n = 7$ slices from 5 mice, 6 slices from 4 mice, and 7 slices from 5 mice). **g** Correlation plot of the density of WFA + PV+ neurons against the magnitude of LTD measured at 50–60 min after LFS at P14, P20, and P28. These data include mice in **f**. The line is the best fit using the least squares regression method ($r = 0.99$, $p = 0.045$). Data represent the mean ± SEM. $^*p < 0.05$ and $^{**}p < 0.01$. n.s., not statistically different

slices in the presence of mGluR5 antagonist MPEP (10 μM; Tocris) (Fig. 4d, f). Additionally, it was reported that manipulations of extracellular concentration of Ca^{2+} and Mg^{2+} can result in LTD induction in slices from adult animals [6, 44]. We therefore examined the effect of increasing extracellular Ca^{2+} level (from 2.5 to 4.0 mM) on LFS-LTD induction. We found that LTD was unmasked in slices from adult mice when slices were perfused with aCSF with high (4.0 mM) Ca^{2+}. Notably, the magnitude of LFS-LTD was virtually identical between vehicle- and ChABC-treated slices in a high Ca^{2+} aCSF condition. The effect of ChABC was occluded, and no further depression was observed (Fig. 4e, f).

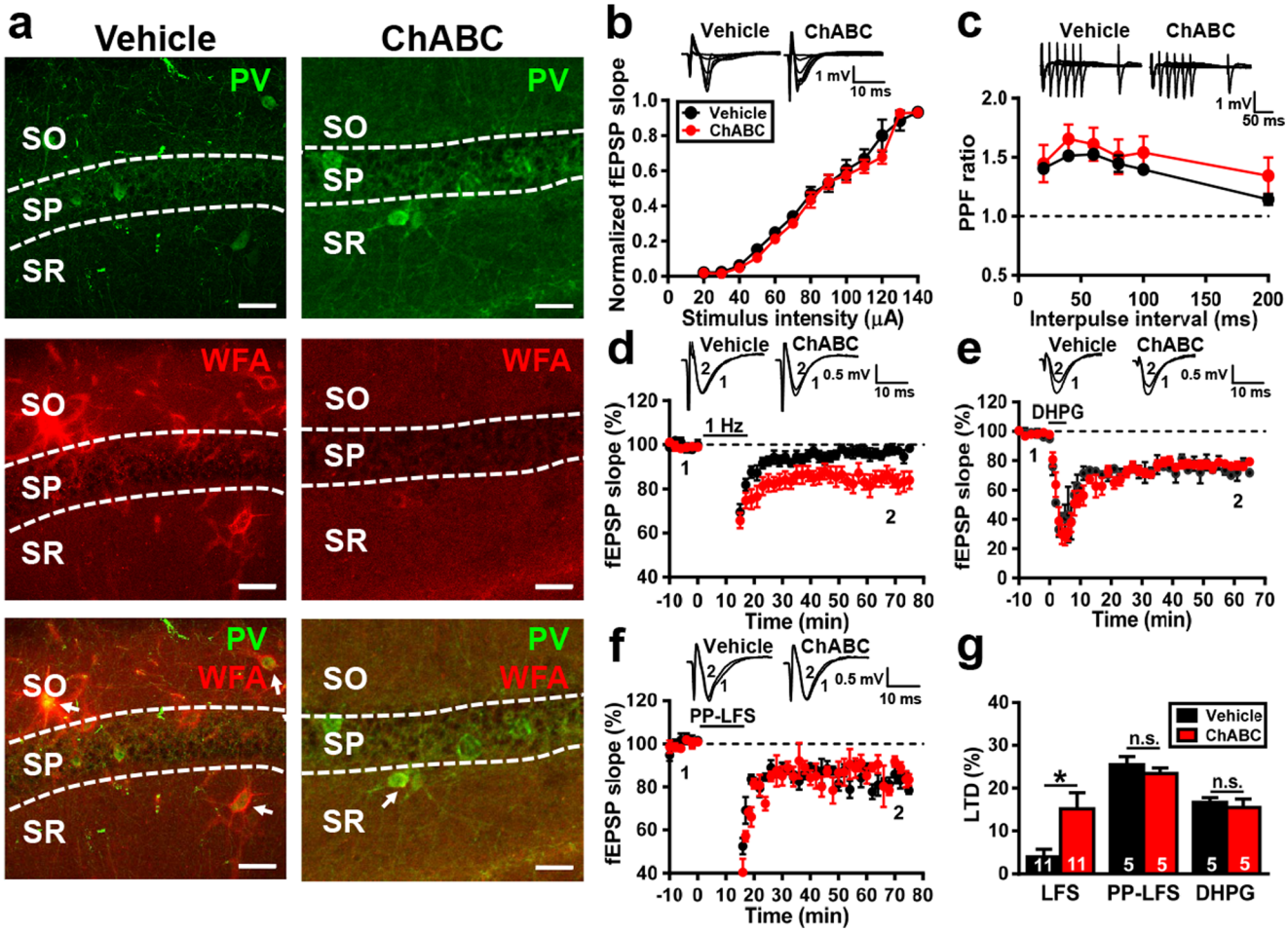

Fig. 3 Disruption of PNNs specifically enhances LFS-LTD. **a** Representative immunofluorescence images showing double fluorescence for PV (green) and WFA (red) in the CA1 region of vehicle (0.1% BSA)- or ChABC (0.2 U/ml in 0.1% BSA)-treated slices from adult mice. Arrows point to double-labeled cells. Scale bar, 40 μm. **b** Input-output curve of normalized fEPSP slope versus stimulus intensity (μA) at Schaffer collateral-CA1 synapses in vehicle- and ChABC-treated slices from adult mice (two-way repeated measures ANOVA, interaction, $F_{(12,89)} = 0.42$, $p = 0.95$, $n = 4$ slices from 4 mice for each group). **c** Comparison of PPF ratio of fEPSPs at Schaffer collateral-CA1 synapses in vehicle- and ChABC-treated slices from adult mice (two-way repeated measures ANOVA, interaction, $F_{(5,42)} = 0.20$, $p = 0.96$, $n = 4$ slices from 4 mice for each group). **d** Summary of experiments showing the induction of LFS-LTD in vehicle- and ChABC-treated slices from adult mice. **e** Summary of experiments showing the induction of LTD by bath application of DHPG (50 μM) for 5 min in vehicle- and ChABC-treated slices from adult mice. **f** Summary of experiments showing the induction of LTD by PP-LFS (40 ms interpulse interval) at 1 Hz for 15 min in the presence of APV (50 μM) in vehicle- and ChABC-treated slices from adult mice. **g** Summary bar graphs comparing average magnitudes of LFS-, PP-LFS-, and DHPG-induced LTD in vehicle- and ChABC-treated slices from adult mice slices. The magnitude of LTD was measured at 50–60 min after LFS (Mann-Whitney *U* test, $p = 0.04$, $n = 11$ slices from 6 mice for each group), PP-LFS (Mann-Whitney *U* test, $p = 0.55$, $n = 5$ slices from 5 mice for each group), and DHPG washout (Mann-Whitney *U* test, $p = 0.55$, $n = 5$ slices from 5 mice for each group). These data include mice in **d**–**f**. Representative traces of fEPSPs were taken at the time indicated by number. *Dash lines* show level of baseline. Data represent the mean ± SEM. *$p < 0.05$ compared with vehicle. n.s., not statistically different

Early-Life Bumetanide Treatment Impairs the Maturation of PNNs and Enhances LFS-LTD at P28

Interfering with the early depolarizing effect of GABA with the NKCC1 inhibitor bumetanide has been shown to impair the maturation of PNNs and prolong critical period plasticity [25]. To further strengthen the relationship between PNNs and LFS-LTD, we investigated whether perinatal interference with normal development of PNNs may affect the time course of the critical period for LTD induction at Schaffer collateral-CA1 synapses. Early-life NKCC1 inhibitor bumetanide treatment has been found to impair PNN development around PV+ interneurons in the visual cortex [25]. To test whether PNNs are similarly modulated by early-life bumetanide treatment in the hippocampal CA1 region, we treated mouse pups with bumetanide (0.2 mg/kg body weight, intraperitoneal administration, twice daily) from P3 to P8 (Fig. 5a). In line with previous findings in the visual cortex [25], we found that hippocampal slices derived from bumetanide-treated mice showed a lower density of WFA+ neurons in the hippocampal CA1 region compared to slices from vehicle controls at P28 (Fig. 5b, c). There was no significant difference in the density

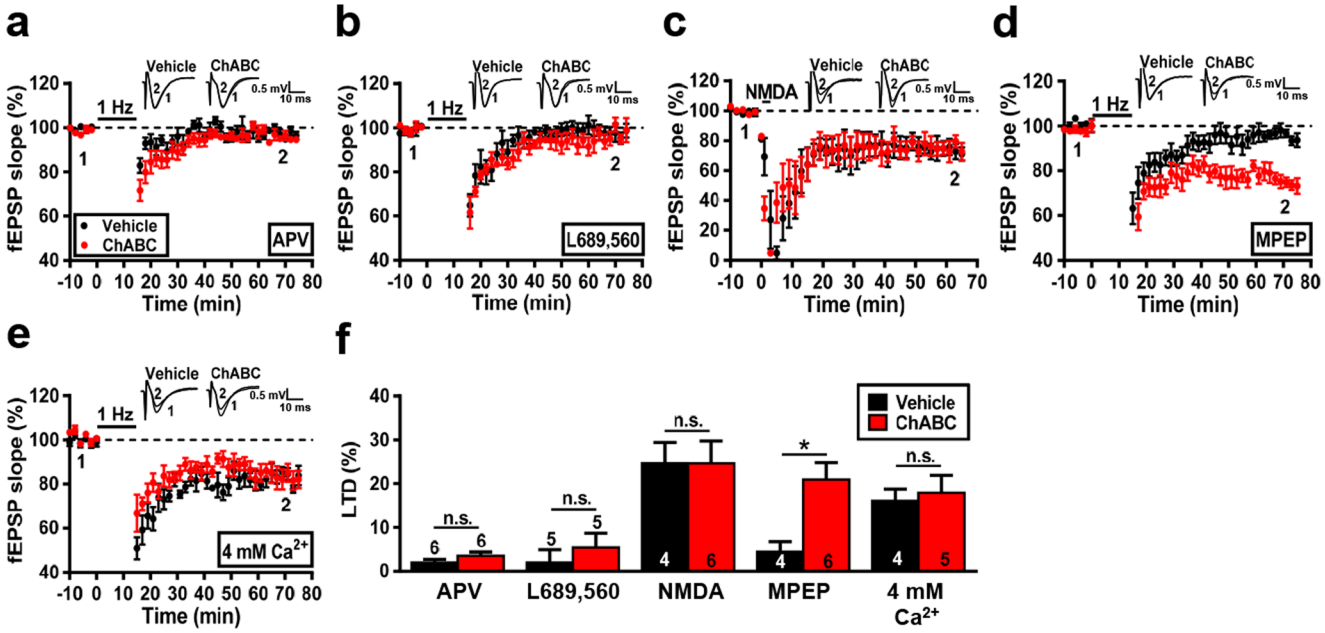

Fig. 4 LFS-LTD in ChABC-treated slices depends on activation of NMDARs. **a** Summary of experiments showing the induction of LFS-LTD in the presence of APV (50 μM) in vehicle- and ChABC-treated slices from adult mice. APV was present throughout the entire recording period. **b** Summary of experiments showing the induction of LFS-LTD in the presence of L689,560 (10 μM) in vehicle- and ChABC-treated slices from adult mice. L689,560 was present throughout the entire recording period. **c** Summary of experiments showing the induction of LTD by bath application of NMDA (15 μM) for 3 min in vehicle- and ChABC-treated slices from adult mice. **d** Summary of experiments showing the induction of LFS-LTD in the presence of MPEP (10 μM) in vehicle- and ChABC-treated slices from adult mice. MPEP was present throughout the entire recording period. **e** Summary of experiments showing the induction of LFS-LTD in 4 mM Ca^{2+} aCSF in vehicle- and ChABC-treated slices from adult mice. **f** Summary bar graphs comparing averaged magnitudes of LFS- or NMDA-induced LTD with different pharmacological treatments in vehicle- and ChABC-treated slices from adult mice slices. The magnitude of LTD was measured at 50–60 min after LFS in the presence of APV (Mann-Whitney *U* test, $p = 0.13$, $n = 6$ slices from 4 mice for each group), L689,560 (Mann-Whitney *U* test, $p = 0.55$, $n = 5$ slices from 4 mice for each group), MPEP (Mann-Whitney *U* test, $p = 0.03$, $n = 4$ slices from 4 mice and 6 slices from 5 mice), and 4 mM Ca^{2+} ACSF (Mann-Whitney *U* test, $p = 0.98$, $n = 4$ slices from 4 mice and 5 slices from 4 mice). The magnitude of NMDA-induced LTD was measured at 50–60 min after NMDA washout (Mann-Whitney *U* test, $p = 0.90$, $n = 4$ slices from 4 mice and 6 slices from 4 mice). These data include mice in **a**–**e**. Representative traces of fEPSPs were taken at the time indicated by number. *Dash lines* show level of baseline. Data represent the mean ± SEM. *$p < 0.05$ compared with vehicle. n.s., not statistically different

of PV+ neurons between the two groups (Fig. 5b, d). Double labeling for WFA and PV confirmed that a lower density of PV+ neurons was surrounded by PNNs in slices from bumetanide-treated mice compared to those from vehicle-treated mice (Fig. 5b, e). Supporting the notion that PNNs restrict LFS-LTD, we found that slices from bumetanide-treated mice displayed significant higher levels of LFS-LTD at Schaffer collateral-CA1 synapses than those from vehicle-treated mice at P28 (Fig. 5f, g).

PNN Disruption Shifts the Excitatory/Inhibitory Synaptic Balance in CA1 Pyramidal Neurons

Finally, we examined how PNN disruption enables LFS to induce LTD at Schaffer collateral-CA1 synapses. Given that PNNs mainly surround PV+ interneurons that participate in the maintenance of the excitatory/inhibitory (E/I) synaptic balance in CA1 pyramidal neurons [45, 46], we hypothesized that PNN disruption may alter the E/I synaptic balance in CA1 pyramidal neurons, which in turn promote LTD induction. To test this, we applied whole-cell patch-clamp recordings to visually identified CA1 pyramidal neurons in slices incubated with vehicle or ChABC for 2 h. Biocytin was routinely added to the pipette solution to retrospectively identify recorded neurons (Fig. 6a). We found that the neuronal excitability of CA1 neurons by quantifying the firing frequency of action potentials to depolarizing current pulses injected into the soma with varying intensities was not altered by ChABC treatment compared to vehicle treatment (Fig. 6a). We next quantified the E/I ratio by measuring the peak amplitude of the excitatory and inhibitory components of the compound evoked synaptic response in vehicle- and ChABC-treated slices. Stimulation in the SP or SR generates a compound EPSC/IPSC in CA1 pyramidal neurons, and each component can be isolated by holding the recorded neuron at the IPSC (0 mV) and EPSC (− 65 mV) reversal potentials, respectively (Fig. 6b). While the amplitudes of EPSCs evoked by either SP or SR stimulation showed no difference between vehicle- and ChABC-treated slices (Fig. 6c), the amplitudes of IPSCs evoked by either SP or SR stimulation were

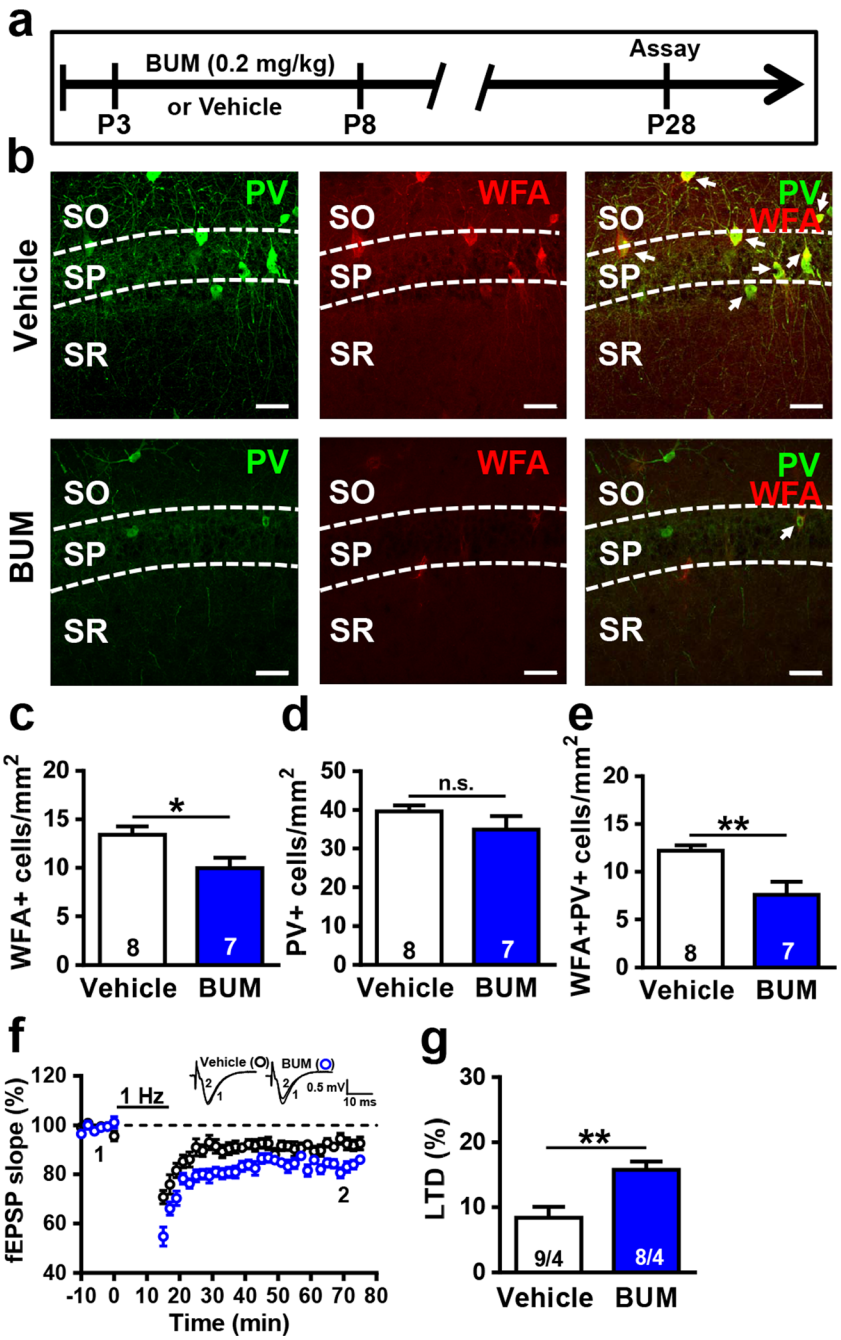

Fig. 5 Early-life bumetanide treatment impairs the maturation of PNNs and enhances LFS-LTD. **a** Schematic representation of the experimental design. Male littermates were injected intraperitoneally twice daily, from P3 to P8, with vehicle (0.01% DMSO in physiological solution) or bumetanide (0.2 mg/kg body weight), and mice were sacrificed for immunohistochemical examination and electrophysiological recordings at P28. Arrows point to double-labeled cells. **b** Representative immunofluorescence images showing double fluorescence for PV (green) and WFA (red) in the CA1 region of hippocampal slices from vehicle- or bumetanide-treated mice. Scale bar, 40 μm. **c**–**e** Bar graph showing the densities of **c** WFA+ (unpaired two-tailed Student's *t* test, $t_{(13)} = 2.81$, $p = 0.01$, $n = 8, 7$); **d** PV+ (unpaired two-tailed Student's *t* test, $t_{(13)} = 1.31$, $p = 0.21$, $n = 8, 7$); and **e** WFA + PV+ neurons (unpaired two-tailed Student's *t* test, $t_{(13)} = 3.26$, $p = 0.006$, $n = 8, 7$) in the CA1 region of hippocampal slices from vehicle- or bumetanide-treated mice at P28. **f** Upper panel: representative traces of fEPSPs were taken at the time indicated by number. Summary of experiments showing the induction of LFS-LTD in slices from vehicle- or bumetanide-treated mice at P28. *Dash lines* show level of baseline. **g** Summary bar graphs comparing averaged magnitudes of LFS-LTD in slices from vehicle- or bumetanide-treated mice at P28. The magnitude of LTD was measured at 50–60 min after LFS (Mann-Whitney *U* test, $p = 0.006$, $n = 9$ slices from 4 mice and 8 slices from 4 mice). These data include mice in **a**–**f**. Data represent the mean ± SEM. *$p < 0.05$, ** $p < 0.01$ compared with vehicle. n.s., not statistically different

significantly smaller in ChABC-treated slices than in slices treated with vehicle (Fig. 6d), thereby increasing the E/I ratio in ChABC-treated slices compared to vehicle-treated slices (Fig. 6e). We also found a significant decrease in the frequency of mIPSCs in ChABC-treated slices, whereas mIPSC amplitude remained unchanged (Fig. 6f). These results suggest that PNN disruption decreases the release of GABA at the presynaptic PV+ interneurons onto CA1 pyramidal neurons and, as a consequence, shifts the E/I synaptic balance toward more excitation.

If PNN disruption enables LFS to induce LTD at Schaffer collateral-CA1 synapses through a disinhibition mechanism, $GABA_A$ receptor agonists should block LTD in ChABC-treated slices. We then examined LFS-induced LTD in

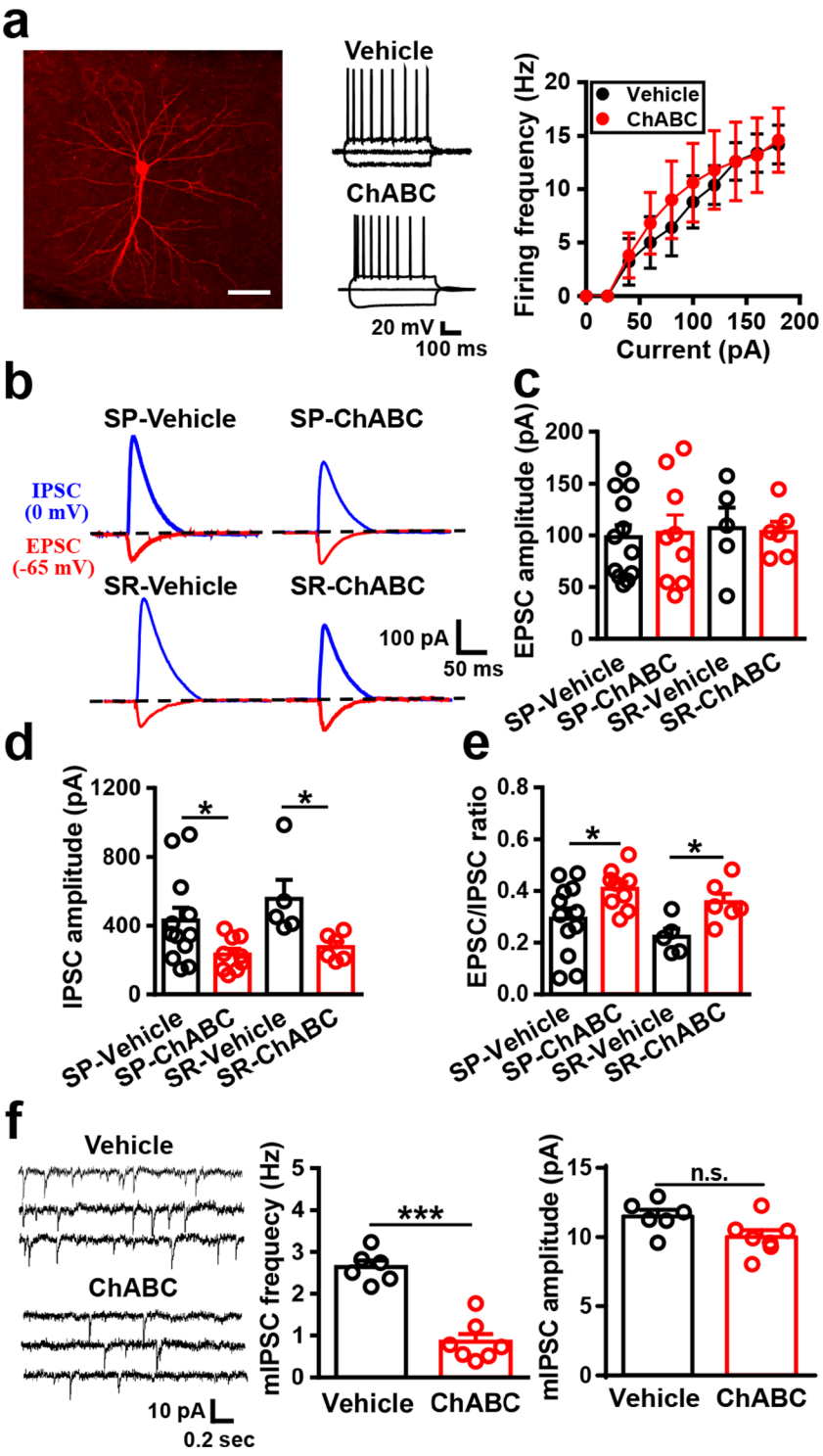

◀ **Fig. 6** Disruption of PNNs shifts the E/I synaptic balance toward more excitation. **a** Left panel: CA1 pyramidal neuron was targeted for recording, filled with biocytin, and reacted with avidin-rhodamine. Scale bar: 50 μm. Middle panel: example traces show electrotonic potential and action potential firing of vehicle- and ChABC-treated CA1 pyramidal neurons (in response to 500 ms long step current injections of − 50 and 100 pA). Right panel: ChABC treatment did not significantly alter action potential firing frequency in response to indicated step current injections (two-way repeated measures ANOVA, interaction, $F_{(14,56)} = 0.35$, $p = 0.98$, $n = 5$ neurons from 4 mice for each group). **b** Representative traces (20 averaged responses in each trace) of isolated inhibitory (IPSC; upward) and excitatory (EPSC; downward) synaptic currents recorded from vehicle- and ChABC-treated CA1 pyramidal neurons at 0 mV and − 65 mV, respectively. Synaptic responses were elicited by electrical stimulation in the SP or SR. **c** Summary bar graphs comparing the amplitudes of EPSCs in vehicle- and ChABC-treated CA1 pyramidal neurons (unpaired two-tailed Student's *t* test, SP: $t_{(19)} = 0.22$, $p = 0.83$, $n = 12$ neurons from 6 mice and 9 neurons from 5 mice; SR: $t_{(9)} = 0.17$, $p = 0.87$, $n = 5$ neurons from 4 mice and 9 neurons from 5 mice). **d** Summary bar graphs comparing the amplitudes of IPSCs in vehicle- and ChABC-treated CA1 pyramidal neurons (unpaired two-tailed Student's *t* test, SP: $t_{(19)} = 2.15$, $p = 0.04$, $n = 12$ neurons from 6 mice and 9 neurons from 5 mice; SR: $t_{(9)} = 2.66$, $p = 0.03$, $n = 5$ neurons from 4 mice and 9 neurons from 5 mice). **e** Summary bar graphs comparing averaged EPSC/IPSC ratio in vehicle- and ChABC-treated CA1 pyramidal neurons (unpaired two-tailed Student's *t* test, SP: $t_{(19)} = 2.24$, $p = 0.04$, $n = 12$ neurons from 6 mice and 9 neurons from 5 mice; SR: $t_{(9)} = 2.92$, $p = 0.02$, $n = 5$ neurons from 4 mice and 9 neurons from 5 mice). **f** Left panel: representative traces of mIPSCs recorded from vehicle- and ChABC-treated CA1 pyramidal neurons at − 60 mV in the presence of TTX (0.5 μM), CNQX (20 μM), and APV (50 μM). Right panel: summary bar graphs depicting the averaged frequency (unpaired two-tailed Student's *t* test, $t_{(11)} = 7.34$, $p < 0.001$, $n = 6$ neurons from 6 mice and 7 neurons from 5 mice) and amplitude (unpaired two-tailed Student's *t* test, $t_{(11)} = 2.18$, $p = 0.052$, $n = 6$ neurons from 6 mice and 7 neurons from 5 mice) of mIPSCs in vehicle- and ChABC-treated CA1 pyramidal neurons. Data represent the mean ± SEM. $^*p < 0.05$ compared with vehicle. n.s., not statistically different

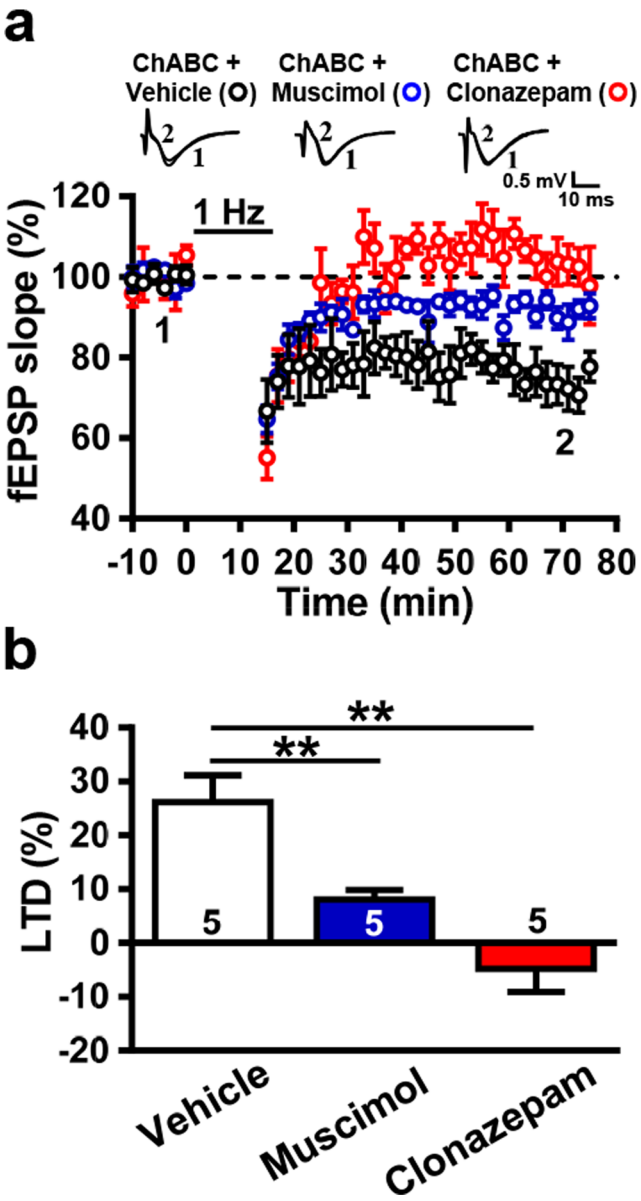

Fig. 7 $GABA_A$ receptor agonists abrogate LFS-induced LTD in ChABC-treated slices. **a** Upper panel: representative traces of fEPSPs were taken at the time indicated by number. Summary of experiments showing the induction of LFS-induced LTD in the presence of vehicle (0.1% DMSO), muscimol (3 μM), or clonazepam (5 μM) in ChABC-treated slices from adult mice. Vehicle, muscimol, or clonazepam was present throughout the entire recording period. *Dash lines* show level of baseline. **b** Summary bar graphs comparing averaged magnitudes of LFS-induced LTD in the presence of vehicle, muscimol, or clonazepam in ChABC-treated slices from adult mice. The magnitude of LTD was measured at 50–60 min after LFS (Mann-Whitney *U* test, vehicle versus muscimol: $p = 0.0079$, $n = 5$ slices from 4 mice for each group; vehicle versus clonazepam: $p = 0.0075$, $n = 5$ slices from 4 mice for each group). These data include mice in **a**. Data represent the mean ± SEM. $^{**}p < 0.01$ compared with vehicle

ChABC-treated slices in the presence of either the $GABA_A$ receptor agonist muscimol or the benzodiazepine agonist clonazepam to counteract the effect of PNN disruption. Consistently, both muscimol (3 μM; Tocris) (Fig. 7a, c) and clonazepam (5 μM; Sigma-Aldrich) (Fig. 7b, c) abrogated LFS-induced LTD in ChABC-treated slices, suggesting that the reduction of GABAergic inhibition contributes mainly to the induction of LFS-LTD in ChABC-treated slices from adult mice.

Discussion

The most striking feature of CA1 LTD is difficult to elicit reliably with the typical LFS in slices from adult animals, which strongly dampens the incentive to elucidate its exact role in learning and memory processes [3, 47]. The prevailing view of age-related changes in LTD induction is that the induction threshold for LTD varies with age. In the present study, we investigated the role of PNNs in age-related decrease in the magnitude of LFS-LTD at Schaffer collateral-CA1 synapses. Our results show a significant inverse correlation between the density of PNN-surrounded PV+ interneurons and the magnitude of LFS-induced LTD in the hippocampal CA1 region during development. Moreover, PNN disruption restores the ability of LFS to induce LTD by

shifting E/I synaptic balance toward more excitation. Altogether, these findings uncovered PNNs as a previously unrecognized negative regulator for LTD induction in the hippocampal CA1 region of adult mice.

Decades of work have consistently reported that LFS becomes less effective to induce LTD with increasing age [8–13]. Rather than a simple loss of LTD induction machinery, previous studies have provided evidence that the LTD intrinsic capacity is intact in the adult hippocampus but obscured by maturation processes. For example, in vitro manipulations of the extracellular Ca^{2+}/Mg^{2+} ratio, as well as the levels of GABA and CaMKII, can result in LTD induction in adult slices [6, 12, 44, 47–49]. Because of the enhancement of LTD induction by $GABA_A$ receptor antagonist in slices from mature animals, Wagner and Alger [47] suggested that developmental differences in LTD induction may result from maturation of GABAergic inhibition, which in turn perturbs NMDAR function. Our study extends this notion by showing, for the first time, that PNN disruption, resulting in a decrease in the level of GABAergic transmission and thereby shifting in the E/I synaptic balance toward more excitation, allowed for the induction of LFS-LTD in slices from adult mice, further confirming that adult CA1 synapses have the cellular machinery for LFS-LTD. More relevant, we have shown that enhancement of $GABA_A$ receptor function abrogates LTD induction in ChABC-treated slices from adult mice, strongly emphasizing GABAergic inhibition as a molecular brake-like factor to limit LTD induction at adult CA1 synapses. In addition, the fact that the inability to induce LFS-LTD at adult CA1 synapses was overcome by elevated extracellular Ca^{2+}/Mg^{2+} ratio strengthens the existing hypothesis that differences in Ca^{2+} regulation may underlie susceptibility to LTD [6, 48, 49]. Along with this hypothesis, we demonstrate that LFS is effective to induce LTD in slices from adult mice under high Ca^{2+} condition. The occlusion of the PNN disruption effect by raising extracellular Ca^{2+} level to 4 mM implies that these two manipulations may share similar mechanisms and that differences in Ca^{2+} regulation may underlie susceptibility to LTD. Moreover, we found that induction of LFS-LTD in ChABC-treated slices from adult mice was blocked by the NMDAR antagonists, APV and L689,560, suggesting that it is not a novel form of LTD. This implies that the induction machinery for LFS-LTD appears to be unchanged at mature synapses. These results give us confidence that PNN disruption results in reduction in GABAergic inhibition on NMDAR activation during LFS, thereby facilitating LFS-LTD induction in adult animals.

Besides contributing to critical period closure [17–20], PNNs also play a role in restricting synaptic plasticity in the adult brain [25–27]. It is generally believed that PNNs drastically limit adult brain plasticity and that they can be degraded to reinstate juvenile-like states of brain plasticity [16]. Consistent with this view, we observed that the timing at which PNN maturation coincides with the reduction in the magnitude of LFS-LTD and PNN disruption enables LFS-LTD in slices from adult animals. Our results also demonstrated that PV+ GABAergic interneurons represent the major neuron population that is enveloped by PNNs in the hippocampal CA1 region. How can disruption of PNNs around PV+ GABAergic interneurons lead to enhance LFS-LTD induction at excitatory synapses on hippocampal CA1 neurons? Given that PNNs likely enwrap glutamatergic inputs along soma and proximal dendrites of PV interneurons [22, 50], one possibility is that PNN disruption reduces the excitability of PV interneurons and thus their ability to inhibit CA1 pyramidal neuron excitability. This disinhibition may lead to increase the extent of NMDAR activation during LFS, which could facilitate induction of NMDAR-dependent LTD. This is in line with finding that $GABA_A$ receptor blockade enhances LFS-LTD in slices from mature rats [47, 51]. This explanation is at variance with conclusions of the earlier studies [21, 22] that implicated increased rather than decreased excitability of PV interneurons when PNNs were lost. One possible reason for the apparent discord is that in the earlier studies, cultured neurons with ChABC treatment or deletion of a PNN component brevican was used, whereas we incubated hippocampal slices with ChABC to remove PNNs; this might have led to ablate PNNs at different levels and therefore differentially affect the intrinsic excitability of PV interneurons. However, our findings are consistent with results from a recent study showing that ChABC treatment reduced the excitability of cortical PV+ fast-spiking interneurons in acute brain slices [23]. Moreover, the fact that the inability to induce LTD at adult synapses can be overcome by increasing extracellular Ca^{2+} levels [6, 48, 49] and the effect of ChABC treatment on LFS-LTD induction is occluded by raising extracellular Ca^{2+} concentration raises an alternative possibility that PNN disruption is sufficient to boost Ca^{2+} signals to levels sufficient to LTD induction by LFS. Furthermore, one might argue that ChABC is not specific to PNNs and digests all chondroitin sulfate glycosaminoglycans. While it could be that ChABC digests other perineuronal/perisynaptic ECM molecules around CA1 pyramidal neurons to alter susceptibility to LTD, we consider this unlikely because ChABC treatment had no effect on basal synaptic transmission and PPF, and the $GABA_A$ receptor agonists abrogated LFS-induced LTD in ChABC-treated slices. Therefore, our results suggest that the action of ChABC treatment is majorly mediated through removal of PNNs around PV interneurons. However, we cannot exclude the possibility that other neuron types were affected by ChABC treatment in our experimental conditions. In contrast to our findings, Bukalo et al. [25] demonstrated that ChABC treatment impaired CA1 LTD induction by LFS (1 Hz for 10 min) in slices from adult mice. Although the reason for this discrepancy in findings is unknown, we noted that different induction protocols were used in the two studies

to elicit LTD. In Bukalo et al.'s study [25], LTD was induced by two trains of LFS at 1 Hz for 10 min (600 pulses) with an intertrain interval of 10 min and the stimulation intensity was increased by 30% when LFS was delivered. However, in our current study, LTD was induced by LFS delivered at 1 Hz for 15 min (900 pulses) at the test pulse intensity. Different LFS paradigms may result in the activation of different cellular processes that may vary in their mode of action. Nonetheless, our findings are consistent with the idea that LFS-LTD is difficult to elicit in hippocampal slices from adult mice [3, 12].

The result showed that there was a significant difference in LTD induction between slices from P20 mice and slices from P28 mice (Fig. 2e, f). Interestingly, other studies have reported that LTD can be consistently induced by LFS at 1 Hz for 15–18 min in hippocampal slices from 1- to 3-month-old C57BL/6J mice [52]. However, Milner et al. [13] showed that hippocampal slices prepared from CBAxC57BL/6 mice aged P28 failed to exhibit a significant LTD by LFS at 1 Hz for 15 min [13], similar to the findings in this study. The reason for these seemingly inconsistent findings is unclear but might be related to differences in growth rates of C57BL/6 mice among different laboratories. Future studies are required to explore this possibility.

Several forms of LTD have been defined by differences in their induction mechanisms [1]. Our data align with the expectation that chemically induced LTD via direct application of NMDA or DHPG is still intact in slices from adult animals [53, 54]. Although chemically induced LTD showed no age dependency and was readily induced in slices from adult mice, we cannot exclude the possibility that a developmental switch in the synaptic mechanisms of LTD exists to accommodate the age-dependent changes in synaptic properties. Indeed, there is evidence that the synaptic mechanisms and protein synthesis dependence of CA1 mGluR-LTD change with developmental age [54]. The fact that ChABC treatment had no effect on the magnitude of NMDA-, DHPG-, and PP-LFS-induced LTD indicates that PNNs specifically restrict LFS-induced LTD at Schaffer collateral-CA1 synapses. One possible explanation for the different effects of PNNs on distinct forms of LTD is likely due to the differential influence of GABAergic inhibition on their induction, as blockade of GABAergic synaptic transmission does not affect DHPG- and PP-LFS-induced LTD at Schaffer collateral-CA1 synapses [55, 56].

NMDARs are heterotetramers composed of two obligatory GluN1 and two GluN2 subunits, with GluN2A and GluN2B being the predominant subunits in the mammalian hippocampus [57]. Importantly, the subunit composition of synaptic NMDARs is not static but changes dynamically during development and in response to neuronal activity and sensory experience. GluN2B-containing NMDARs are expressed predominantly early in development, while the expression of GluN2A-containing NMDARs increases during development [58]. This subunit change thought to regulate developmental changes in the directionality of NMDAR-mediated synaptic plasticity [59, 60]. Given that changes in subunit composition of synaptic NMDARs can be rapid at the adult synapses [61], another interesting consideration is that this subunit change might be reversed by ChABC treatment, which in turn enables the induction of LFS-LTD. Future studies are required to test this possibility.

Mature PNNs are considered to be highly stable structures unless perturbed by brain injury or neurodegenerative diseases [50, 62]. Here we show, for the first time, that early bumetanide treatment impairs the maturation of PNNs and enhances LFS-LTD induction in the hippocampus. Consistently, the same bumetanide treatment regimen also leads to a delayed maturation of PNNs in the developing rat visual cortex [32]. While the mechanism by which bumetanide treatment delays PNN development remains to be determined, a potential mechanism of action of bumetanide is mediated by interfering with GABA-induced depolarization during early development [32]. Our results raise an intriguing possibility that bumetanide treatment blocks the early depolarizing action of GABA to initiate a cascade of molecular events that act to promote PNN development around PV interneurons, reducing GABAergic synaptic activity in CA1 pyramidal neurons and thereby allowing for the induction of LFS-LTD in slices from adult mice. Further studies are required to determine the molecular identity that links GABA-induced depolarization to PNN development.

In summary, we have uncovered a novel mechanism underlying age-related decline in the induction of hippocampal CA1 LTD. Results from this study suggest an unidentified and important role of PNNs in restricting LFS-LTD at mature Schaffer collateral to CA1 synapses. Our results also reveal that PNN disruption restores the ability of LFS to induce LTD at adult synapses by shifting E/I synaptic balance toward more excitation. These findings further increase our understanding of mechanisms by which PNNs control synaptic plasticity in the hippocampus. Assuming that a balance between LTP and LTD may underlie efficient memory storage [63, 64] and NMDAR-dependent LTD is hypothesized to underlie memory flexibility [65], we suggest that further study is warranted to determine whether age-related decline in the magnitude of LTD may contribute to enhance memory stabilization and preservation.

Acknowledgements We thank the technical services provided by the Bio-image Core Facility of the National Core Facility Program for Biotechnology, Ministry of Science and Technology, Taiwan.

Author Contributions G.H.K., Y.T.L., T.C.T., and K.S.H. designed experiments. G.H.K., Y.T.L., and T.C.T. performed experiments and analyzed data. G.H.K., Y.T.L., and K.S.H. wrote the paper.

Funding Information This work was supported by research grants from the National Health Research Institute (NHRI-EX107-10613NI) and the Ministry of Science and Technology (106-2320-B-006-026-MY3 and 107-2320-B-006-037-MY3), Taiwan.

Compliance with Ethical Standards

All experimental procedures were conducted in accordance with the National Institutes of Health guidelines for the care and use of laboratory animals and were approved by the Institutional Animal Care and Use Committee of National Cheng Kung University.

Conflict of Interest The authors declare that they have no conflict of interest.

References

1. Malenka RC, Bear MF (2004) LTP and LTD: an embarrassment of riches. Neuron 44:5–21
2. Kemp A, Manahan-Vaughan D (2007) Hippocampal long-term depression: master or minion in declarative memory processes? Trends Neurosci 30:111–118
3. Pinar C, Fontaine CJ, Triviño-Paredes J, Lottenberg CP, Gil-Mohapel J, Christie BR (2017) Revisiting the flip side: long-term depression of synaptic efficacy in the hippocampus. Neurosci Biobehav Rev 80:394–413
4. Abraham WC (1996) Induction of heterosynaptic and homosynaptic LTD in hippocampal sub-regions *in vivo*. J Physiol Paris 90:305–306
5. Massey PV, Bashir ZI (2007) Long-term depression: multiple forms and implications for brain function. Trends Neurosci 30:176–184
6. Dudek SM, Bear MF (1992) Homosynaptic long-term depression in area CA1 of hippocampus and effects of *N*-methyl-D-aspartate receptor blockade. Proc Natl Acad Sci U S A 89:4363–4367
7. Mulkey RM, Herron CE, Malenka RC (1993) An essential role for protein phosphatases in hippocampal long-term depression. Science 261:1051–1055
8. Fujii S, Saito K, Miyakawa H, Ito K, Kato H (1991) Reversal of long-term potentiation (depotentiation) induced by tetanus stimulation of the input to CA1 neurons of guinea pig hippocampal slices. Brain Res 555:112–122
9. Dudek SM, Bear MF (1993) Bidirectional long-term modification of synaptic effectiveness in the adult and immature hippocampus. J Neurosci 13:2910–2918
10. Bashir ZI, Collingridge GL (1994) An investigation of depotentiation of long-term potentiation in the CA1 region of the hippocampus. Exp Brain Res 100:437–443
11. O'Dell TJ, Kandel ER (1994) Low-frequency stimulation erases LTP through an NMDA receptor-mediated activation of protein phosphatases. Learn Mem 1:129–139
12. Mayford M, Wang J, Kandel ER, O'Dell TJ (1995) CaMKII regulates the frequency-response function of hippocampal synapses for the production of both LTD and LTP. Cell 81:891–904
13. Milner AJ, Cummings DM, Spencer JP, Murphy KP (2004) Bidirectional plasticity and age-dependent long-term depression at mouse CA3-CA1 hippocampal synapses. Neurosci Lett 367:1–5
14. Celio MR, Spreafico R, De Biasi S, Vitellaro-Zuccarello L (1998) Perineuronal nets: past and present. Trends Neurosci 21:510–515
15. Wang D, Fawcett J (2012) The perineuronal net and the control of CNS plasticity. Cell Tissue Res 349:147–160
16. Sorg BA, Berretta S, Blacktop JM, Fawcett JW, Kitagawa H, Kwok JC, Miquel M (2016) Casting a wide net: role of perineuronal nets in neural plasticity. J Neurosci 36:11459–11468
17. Pizzorusso T, Medini P, Berardi N, Chierzi S, Fawcett JW, Maffei L (2002) Reactivation of ocular dominance plasticity in the adult visual cortex. Science 298:1248–1251
18. Barritt AW, Davies M, Marchand F, Hartley R, Grist J, Yip P, McMahon SB, Bradbury EJ (2006) Chondroitinase ABC promotes sprouting of intact and injured spinal systems after spinal cord injury. J Neurosci 26:10856–10867
19. Massey JM, Hubscher CH, Wagoner MR, Decker JA, Amps J, Silver J, Onifer SM (2006) Chondroitinase ABC digestion of the perineuronal net promotes functional collateral sprouting in the cuneate nucleus after cervical spinal cord injury. J Neurosci 26:4406–4414
20. Lensjø KK, Lepperød ME, Dick G, Hafting T, Fyhn M (2017) Removal of perineuronal nets unlocks juvenile plasticity through network mechanisms of decreased inhibition and increased gamma activity. J Neurosci 37:1269–1283
21. Dityatev A, Brückner G, Dityateva G, Grosche J, Kleene R, Schachner M (2007) Activity-dependent formation and functions of chondroitin sulfate-rich extracellular matrix of perineuronal nets. Dev Neurobiol 67:570–588
22. Favuzzi E, Marques-Smith A, Deogracias R, Winterflood CM, Sánchez-Aguilera A, Mantoan L, Maeso P, Fernandes C et al (2017) Activity-dependent gating of parvalbumin interneuron function by the perineuronal net protein brevican. Neuron 95:639–655
23. Balmer TS (2016) Perineuronal nets enhance the excitability of fast-spiking neurons. eNeuro 3:e0112–e0116
24. Gogolla N, Caroni P, Lüthi A, Herry C (2009) Perineuronal nets protect fear memories from erasure. Science 325:1258–1261
25. Bukalo O, Schachner M, Dityatev A (2001) Modification of extracellular matrix by enzymatic removal of chondroitin sulfate and by lack of tenascin-R differentially affects several forms of synaptic plasticity in the hippocampus. Neuroscience 104:359–369
26. Kochlamazashvili G, Henneberger C, Bukalo O, Dvoretskova E, Senkov O, Lievens PM, Westenbroek R, Engel AK et al (2010) The extracellular matrix molecule hyaluronic acid regulates hippocampal synaptic plasticity by modulating postsynaptic L-type Ca^{2+} channels. Neuron 67:116–128
27. Carstens KE, Phillips ML, Pozzo-Miller L, Weinberg RJ, Dudek SM (2006) Perineuronal nets suppress plasticity of excitatory synapses on CA2 pyramidal neurons. J Neurosci 36:6312–6320
28. Ben-Ari Y, Holmes GL (2005) The multiple facets of γ-aminobutyric acid dysfunction in epilepsy. Curr Opin Neurol 18:141–145
29. Ben-Ari Y, Woodin MA, Sernagor E, Cancedda L, Vinay L, Rivera C, Legendre P, Luhmann HJ et al (2012) Refuting the challenges of the developmental shift of polarity of GABA actions: GABA more exciting than ever! Front Cell Neurosci 6:35
30. Sernagor E, Chabrol F, Bony G, Cancedda L (2010) GABAergic control of neurite outgrowth and remodeling during development and adult neurogenesis: general rules and differences in diverse systems. Front Cell Neurosci 4:11
31. Wang DD, Kriegstein AR (2011) Blocking early GABA depolarization with bumetanide results in permanent alterations in cortical circuits and sensorimotor gating deficits. Cereb Cortex 21:574–587
32. Deidda G, Parrini M, Naskar S, Bozarth IF, Contestabile A, Cancedda L (2015) Reversing excitatory $GABA_AR$ signaling restores synaptic plasticity and memory in a mouse model of Down syndrome. Nat Med 21:318–326
33. Yang CH, Huang CC, Hsu KS (2012) A critical role for protein tyrosine phosphatase nonreceptor type 5 in determining individual susceptibility to develop stress-related cognitive and morphological changes. J Neurosci 32:7550–7562

34. Lin YT, Chen CC, Huang CC, Nishimori K, Hsu KS (2017) Oxytocin stimulates hippocampal neurogenesis via oxytocin receptor expressed in CA3 pyramidal neurons. Nat Commun 8:537
35. Ueno H, Suemitsu S, Okamoto M, Matsumoto Y, Ishihara T (2017) Parvalbumin neurons and perineuronal nets in the mouse prefrontal cortex. Neuroscience 343:115–127
36. Huang CC, Hsu KS (2010) Activation of muscarinic acetylcholine receptors induces a nitric oxide-dependent long-term depression in rat medial prefrontal cortex. Cereb Cortex 20:982–996
37. Huang CC, Yeh CM, Wu MY, Chang AY, Chan JY, Chan SH, Hsu KS (2011) Cocaine withdrawal impairs metabotropic glutamate receptor-dependent long-term depression in the nucleus accumbens. J Neurosci 31:4194–4203
38. Yamada J, Ohgomori T, Jinno S (2015) Perineuronal nets affect parvalbumin expression in GABAergic neurons of the mouse hippocampus. Eur J Neurosci 41:368–378
39. McRae PA, Baranov E, Sarode S, Brooks-Kayal AR, Porter BE (2010) Aggrecan expression, a component of the inhibitory interneuron perineuronal net, is altered following an early-life seizure. Neurobiol Dis 39:439–448
40. Yamada J, Jinno S (2013) Spatio-temporal differences in perineuronal net expression in the mouse hippocampus, with reference to parvalbumin. Neuroscience 253:368–379
41. Kemp N, McQueen J, Faulkes S, Bashir ZI (2000) Different forms of LTD in the CA1 region of the hippocampus: role of age and stimulus protocol. Eur J Neurosci 12:360–366
42. Kwok JC, Dick G, Wang D, Fawcett JW (2011) Extracellular matrix and perineuronal nets in CNS repair. Dev Neurobiol 71:1073–1089
43. Lee HK, Kameyama K, Huganir RL, Bear MF (1998) NMDA induces long-term synaptic depression and dephosphorylation of the GluR1 subunit of AMPA receptors in hippocampus. Neuron 21:1151–1162
44. Dudek SM, Bear MF (1993) Bidirectional long-term modification of synaptic effectiveness in the adult and immature hippocampus. J Neurosci 13:2910–2918
45. Lee SH, Marchionni I, Bezaire M, Varga C, Danielson N, Lovett-Barron M, Losonczy A, Soltesz I (2014) Parvalbumin-positive basket cells differentiate among hippocampal pyramidal cells. Neuron 82:1129–1144
46. Horn ME, Nicoll RA (2018) Somatostatin and parvalbumin inhibitory synapses onto hippocampal pyramidal neurons are regulated by distinct mechanisms. Proc Natl Acad Sci U S A 115:589–594
47. Wagner JJ, Alger BE (1995) GABAergic and developmental influences on homosynaptic LTD and depotentiation in rat hippocampus. J Neurosci 15:1577–1586
48. Norris CM, Korol DL, Foster TC (1996) Increased susceptibility to induction of long-term depression and long-term potentiation reversal during aging. J Neurosci 16:5382–5392
49. Foster TC, Kumar A (2007) Susceptibility to induction of long-term depression is associated with impaired memory in aged Fischer 344 rats. Neurobiol Learn Mem 87:522–535
50. Sun ZY, Bozzelli PL, Caccavano A, Allen M, Balmuth J, Vicini S, Wu JY, Conant K (2018) Disruption of perineuronal nets increases the frequency of sharp wave ripple events. Hippocampus 28:42–52
51. Kerr DS, Abraham WC (1995) Cooperative interactions among afferents govern the induction of homosynaptic long-term depression in the hippocampus. Proc Natl Acad Sci U S A 92:11637–11641
52. Stevens CF, Tonegawa S, Wang Y (1994) The role of calcium-calmodulin kinase II in three forms of synaptic plasticity. Curr Biol 4:687–693
53. Kamal A, Ramakers GM, Urban IJ, De Graan PN, Gispen WH (1999) Chemical LTD in the CA1 field of the hippocampus from young and mature rats. Eur J Neurosci 11:3512–3516
54. Kumar A, Foster TC (2007) Shift in induction mechanisms underlies an age-dependent increase in DHPG-induced synaptic depression at CA3 CA1 synapses. J Neurophysiol 98:2729–2736
55. Palmer MJ, Irving AJ, Seabrook GR, Jane DE, Collingridge GL (1997) The group I mGlu receptor agonist DHPG induces a novel form of LTD in the CA1 region of the hippocampus. Neuropharmacology 36:1517–1532
56. Rohde M, Tokay T, Köhling R, Kirschstein T (2009) $GABA_A$ receptor inhibition does not affect mGluR-dependent LTD at hippocampal Schaffer collateral-CA1 synapses. Neurosci Lett 467:20–25
57. Paoletti P, Bellone C, Zhou Q (2013) NMDA receptor subunit diversity: impact on receptor properties, synaptic plasticity and disease. Nat Rev Neurosci 14:383–400
58. Sans N, Petralia RS, Wang YX, Blahos J 2nd, Hell JW, Wenthold RJ (2000) A developmental change in NMDA receptor-associated proteins at hippocampal synapses. J Neurosci 20:1260–1271
59. Yashiro K, Philpot BD (2008) Regulation of NMDA receptor subunit expression and its implications for LTD, LTP, and metaplasticity. Neuropharmacology 55:1081–1094
60. Gray JA, Shi Y, Usui H, During MJ, Sakimura K, Nicoll RA (2011) Distinct modes of AMPA receptor suppression at developing synapses by GluN2A and GluN2B: single-cell NMDA receptor subunit deletion *in vivo*. Neuron 71:1085–1101
61. Bellone C, Nicoll RA (2007) Rapid bidirectional switching of synaptic NMDA receptors. Neuron 55:779–785
62. Fawcett JW (2015) The extracellular matrix in plasticity and regeneration after CNS injury and neurodegenerative disease. Prog Brain Res 218:213–226
63. Ahmadian G, Ju W, Liu L, Wyszynski M, Lee SH, Dunah AW, Taghibiglou C, Wang Y et al (2004) Tyrosine phosphorylation of GluR2 is required for insulin-stimulated AMPA receptor endocytosis and LTD. EMBO J 23:1040–1050
64. Liu L, Wong TP, Pozza MF, Lingenhoehl K, Wang Y, Sheng M, Auberson YP, Wang YT (2004) Role of NMDA receptor subtypes in governing the direction of hippocampal synaptic plasticity. Science 304:1021–1024
65. Nicholls RE, Alarcon JM, Malleret G, Carroll RC, Grody M, Vronskaya S, Kandel ER (2008) Transgenic mice lacking NMDAR-dependent LTD exhibit deficits in behavioral flexibility. Neuron 58:104–117